UNIVERSITÀ DEGLI STUDI DI PADOVA

SCHOOL OF SCIENCE

Department of
Geoscience

MASTERS THESIS IN GEOPHYSICS FOR NATURAL RISKS
ANDRESOURCES

The use of multiple-gradient array for electrical resistivity tomography

Supervisor: Prof. Jacopo Boaga

Co-supervisor: Dr. Luca Peruzzo

Graduating student: Navid Ebrahimi

Academic Year 2022/2023

Abstract

This thesis delves into the application of the Syscal Terra electrical resistivity meter with a multiple-gradient array for subsurface imaging, with a specific focus on the Experimental Farm "L. Toniolo" at the University of Padova in Legnaro, North-Eastern Italy. The study area features Fluvi-Calcaric Cambisol soil, characteristic of the Venetian plain, with low natural fertility. The Syscal Terra, equipped with 20 measurement channels, is employed for efficient data acquisition, providing high-resolution resistivity and data at varying depths. Surveys were conducted using dipole-dipole and multiple-gradient arrays along a 14.2 m transect line with 72 stainless-steel electrodes spaced at 0.2 m intervals. The instrument's design, including a large built-in touchscreen display and high-power capabilities (up to 10000 V), enhances ease of use and field deployment. The use of Li batteries allows for international transport convenience, and the unit's functionality can be easily verified with built-in test procedures. The acquired data underwent inversion processing with the ResIPy software, employing the R2 code based on Occam's inversion method. The resulting electrical resistivity tomography (ERT) images provide detailed insights into the subsurface structure in 2D. Various electrode arrays, such as multiple-gradient, square, dipole-dipole, Wenner, and Schlumberger, were discussed, with the emphasis on the multiple-electrode gradient survey. ERT proves to be a valuable geophysical tool, offering efficient imaging of complex geological features. The technique has been successfully applied to investigate areas with diverse geological characteristics, including volcanic and geothermal regions, landslides, seismotectonic structures, hydro-geological phenomena, and

environmental issues. Innovations in inversion methods, incorporating topography, contribute to accurate data interpretation, aiding in the resolution of complex geological problems. This thesis concludes by highlighting the significance of the multiple-gradient array in electrical resistivity tomography, showcasing its role in advancing our understanding of subsurface geological features. The research presented contributes valuable insights to the field, demonstrating the effectiveness of the technology in various geological contexts.

Acknowledgements

I extend my sincere gratitude to Prof. Jacopo Boaga, whose guidance, expertise, and unwavering support have been instrumental throughout the research and completion of this thesis. Prof. Boaga's mentorship has not only shaped the academic aspects of this work but has also fostered my growth as a researcher.

I would like to express my heartfelt appreciation to Dr. Luca Peruzzo, whose valuable assistance and insightful contributions significantly enriched the development of this thesis. Dr. Peruzzo's dedication to fostering academic excellence and his willingness to share knowledge have been invaluable in the realization of this research endeavor.

I am deeply thankful to my family for their unwavering support, encouragement, and understanding throughout this academic journey. Their belief in my abilities and their constant encouragement provided the motivation needed to overcome challenges and persevere in the pursuit of knowledge.

This work would not have been possible without the support of Prof. Boaga, Dr. Peruzzo, and my family. Their contributions, both academic and personal, have played a pivotal role in the successful completion of this thesis.

Contents

List of Figures

Fig 14: depicts the parameterization of a specific subset within the structured finite element mesh. The grey lines represent the finite element mesh, while the black lines outline the designated parameter zones.

Fig 15: illustrates the parameterization of an unstructured mesh as defined in mesh.dat. The grey lines represent the finite element mesh, and the black lines indicate the boundaries of the designated parameters.

Fig 16: The mesh.dat file defines the parameter and zone for each element, providing comprehensive control over the parameterization process.

Fig 17: displays zoning for parameterization in an unstructured triangular mesh, with distinct colors representing different parameter zones.

Fig 18: Top View of the Syscal terra unit including the colour display, keypad and ports (Image courteously provided by Iris Instruments)

Fig 19: Comparison of 2D Sensitivity Sections: multiple-gradient Array vs. Dipole-Dipole Configuration for Subsurface Investigations Related to Field Dataset.

Fig 20: Comparison of 2D inverted models: multiple-gradient Array vs. Dipole-Dipole Configuration for Subsurface Investigations Related to Field Dataset.

Fig 21: 2D Mesh Plot Displaying Contrasting Resistivity Layers: Conductive Layer (50 ohm.m) Positioned at 2.5 to 3m Depth Against Background Lithology (500 ohm.m).

Fig 22: Comparative 2D synthetic sections: Synthetic Subsurface Investigations Using multiple-gradient Array vs. Dipole-Dipole Configuration.

Fig 23: Comparative 2D inverted model: Synthetic Subsurface Investigations Using multiple-gradient Array vs. Dipole-Dipole Configuration.

List of Tables

1.1 Aims and Objectives

The study aims to evaluate and compare the performance of different electrode arrays, including the multiple-gradient and dipole-dipole arrays, within the specific geological context of the Experimental Farm "L. Toniolo" at the University of Padova in Legnaro, North-Eastern Italy. This evaluation aims to ascertain the efficacy and practical applicability of these arrays for subsurface imaging in Fluvi-Calcaric Cambisol soil. By conducting a detailed comparative analysis, the study seeks to determine the strengths and weaknesses of each array in providing accurate and detailed subsurface information. This comparison aims to refine the understanding of the most suitable and reliable method for geological mapping and subsurface structure interpretation within this distinct geological setting. The following represent the study's objectives:

- Field Study and Site-Specific Data Acquisition: Execute surveys utilizing the Syscal Terra with 20 measurement channels, employing multiple electrode arrays within the Experimental Farm "L. Toniolo" in Legnaro, North-Eastern Italy, focusing on the characteristics of Fluvi-Calcaric Cambisol soil.

- Data Processing and Imaging Techniques: Utilize ResIPy software with inversion methods based on Occam's inversion principle (R2/R3t codes) to process resistivity, generating detailed 2D and electrical resistivity tomography (ERT) images specifically for the Legnaro site.

- Comparison and Validation: Compare the outcomes from multiple-gradient and dipole-dipole arrays within the Legnaro site, validating results against numerical modeling

outcomes and field data, specifically focusing on the unique geological characteristics of the location.

- Refinement of Plotting and Quality Assessment: Evaluate the proposed pseudosection plotting formulas for assessing data quality within the Legnaro site, refining techniques for distinct parameter assessments such as m-factor or a-spacing to enhance accuracy in data interpretation.

- Site-Specific Advantages and Limitations Analysis: Assess the suitability of each electrode array (multiple-gradient, dipole-dipole) within the Legnaro site, considering factors such as data acquisition speed, density, noise sensitivity, and logistical feasibility.

- Contribution to Local Geophysical Understanding: Emphasize the significance of the multiple-gradient array in enhancing the understanding of subsurface features within the Legnaro site, contributing insights to the field of geophysical investigations in the North-Eastern Italian region.

2.0 Physical Principles of ERT Methods

In this section, we will begin by outlining the primary electrical prospecting methods, delving into their potential applications, as well as examining the advantages and drawbacks associated with each. Following this, we will shift our attention to the Electrical Resistivity Tomography (ERT) technique, which is the primary focus of this thesis. We will explore the principles underlying ERT and its relevance to the research objectives. Concluding the chapter, we will elaborate on the methodologies employed for data acquisition, along with additional insights pertaining to the investigated area.

2.1 General information on electrical methods

Geophysics employs indirect, non-destructive, and swift analysis methods to examine various physical properties of the subsurface. Each geophysical method is tailored to investigate a specific soil parameter. Consequently, the selection of the investigative approach aligns with the study's objectives. In comparison to other direct and point-specific techniques in the geological field, geophysical investigations yield areal data, effectively revealing spatial variations in the studied property. Geophysical measurement methods can be categorized into active ones, necessitating an artificial signal source to measure the pertinent physical parameter, and passive ones, capitalizing on the naturally occurring Earth fields.

Direct current techniques (DC Methods) offer a swift, non-intrusive, and relatively cost-effective means to explore the first few meters of the subsurface, revealing the spatial arrangement of electrical resistivity or electrical conductivity. These properties are

contingent on lithology, soil fluid content, and chemistry. The methodology involves employing an artificial source of direct current to introduce a signal into the ground, coupled with the measurement of the potential difference experienced by the signal along its trajectory. Typically, two metal rods serve as energizing electrodes to introduce the current, while a second pair of electrodes, termed potentiometric electrodes, measures the potential difference. The investigative approach adheres to Ohm's law, enabling the reconstruction of current flow paths and the determination of variations in electrical resistivity distribution underground.

These investigation techniques can be employed across various geological scenarios. Some common applications include:

- Identifying preferred pathways for groundwater flow

- Conducting archaeological studies

- Detecting buried structures

- Locating faults and discontinuities

- Monitoring environmental conditions

- Determining the depth of bedrock

- Locating underground cavities

Electric methods find widespread application due to their use of cost-effective and sturdy instrumentation, suitable for both surface and borehole applications. The utilization of electrical methods in investigations is straightforward and expeditious, yielding results with extensive areal coverage and effective penetration. The associated data processing programs are sophisticated yet user-friendly. The correlation between measured electrical resistivity

values and changes in water content and salinity has been well-established through numerous studies, although local calibrations may be necessary due to the impact of specific subsoil parameters.

Conversely, the data gathered are susceptible to surface variations and experience a decrease in resolution as depth increases. These methods are more commonly utilized in easily reachable environments due to the necessity for effective coupling between electrodes and the ground, as well as extended investigation periods. The use of borehole applications proves beneficial in enhancing depth resolution, albeit demanding appropriate instrumentation.

The field of electrical acquisitions has witnessed significant advancements since the 1980s, marked by the introduction of multi-electrode instruments alongside the initial implementation of numerical inversion and graphical data representation programs. Specifically, techniques such as electrical resistivity tomography (ERT) have been devised, utilizing an array of numerous electrodes connected to the georesistivimeter via multi-channel cables. This setup facilitates the rapid and automated collection of apparent resistivity values for all possible quadruples generated by the combination of electrodes positioned on the surface. ERT acquisitions enable the generation of 2D and 3D images illustrating variations in a specific physical property within the investigated space. Furthermore, technological progress in these methods has enabled the examination of time-lapse phenomena.

Electrical Resistivity Tomography (ERT) functions based on the fundamental principles outlined in Ohm's law, as expressed in the equation:

$$V = I \ R$$

where V denotes electric voltage, I signifies the injected current, and R represents resistance. The determination of resistance in the context of a cylindrical object with dimensions length (L) and cross-sectional area (A) is articulated by the formula:

$$R = \frac{\rho L}{A}$$

where ρ is the material's electrical resistivity. It is crucial to underscore that electrical resistivity is an inherent material property, impervious to variations in current intensity or electrode array geometry and is inversely proportional to electrical conductivity ($\rho = \sigma^{-1}$).

The soil's resistivity is primarily contingent on its compositional features, including grain size, shape, and grain porosity, as well as the presence and chemistry of interstitial fluids. Pure water, for instance, exhibits minimal conductivity, but the inclusion of dissolved salts contributes to its conductivity. Archie's law, which articulates this relationship, is characterized by the empirical formula:

$$F = a\Phi^{-m}$$

Where S represents the water-saturated porous fraction, n is an empirical coefficient, and F is termed the formation factor. The formation factor, in turn, relies on the porosity ϕ, the soil's cementation rate m, and the empirical factor a associated with the lithology:

$$\rho = \rho_w F S_n$$

It is evident that the saturation component is the sole variable in the formula, with the other parameters being tied to the geological characteristics of the medium, which remain constant over time. The average electrical resistivity values, indicative of different soil types, may undergo

changes in the presence of organic matter and show fluctuations based on salinity and saturation rates. To illustrate, freshwater typically exhibits electrical resistivity values ranging from 10 to 100 Ω m, whereas seawater generally does not surpass 0.2 Ω m.

Consistent with the outcomes of particular investigations undertaken by Carbognin et al. (2004), de Franco et al. (2009), Viezzoli et al. (2010), Teatini et al. (2011), and Da Lio et al. (2013), the defined electrical resistivity values for the lower limit of brackish water and the upper limit of freshwater are below 5 Ω m and above 10 Ω m, respectively. This nuanced comprehension emphasizes the significance of electrical resistivity in delineating variations in subsurface conditions within the domain of geophysical and environmental studies.

In the extensive inquiries carried out by Binley and Kemna (2005) and Binley (2015), the examination revolves around an isotropic three-dimensional (3-D) electrical resistivity distribution represented as $\rho(x, y, z)$. In this framework, the derivation of the 3-D electric potential, $V(x, y, z)$, resulting from the injection of current I at a known position, is clarified by employing Poisson's equation:

$$\nabla.\left(\frac{1}{\rho} \nabla V\right) = -I\delta(x)$$

In this context, the nabla operator ($\nabla=\partial/\partial x, \partial/\partial y, \partial/\partial z$) is utilized, and δ represents the Dirac delta function. The boundary conditions for Equation 2.3 are specified as follows:

Dirichlet boundary conditions:

$$V(r\rightarrow\infty)=0$$

where r= $\sqrt{x2 + y2 + z2}$ and z≤0.

Neumann boundary conditions:

$$\sigma \frac{\partial V}{\partial x}\bigg|_{x \to x_0} = I_0$$

Where r denotes the distance from the current source, and I_0 represents the imposed current flux at the boundary.

In the initial examination of the equation, two current electrodes are introduced, injecting current I from the ground surface, with one electrode positioned at an infinite distance (refer to Figure). Assuming a homogeneous resistivity distribution and the existence of a current sink at infinity, the resulting solution is articulated as:

$$V(r) = \frac{I\rho}{2\pi r}$$

An essential aspect to take into account is the semi-infinite nature of the domain for z≤0.
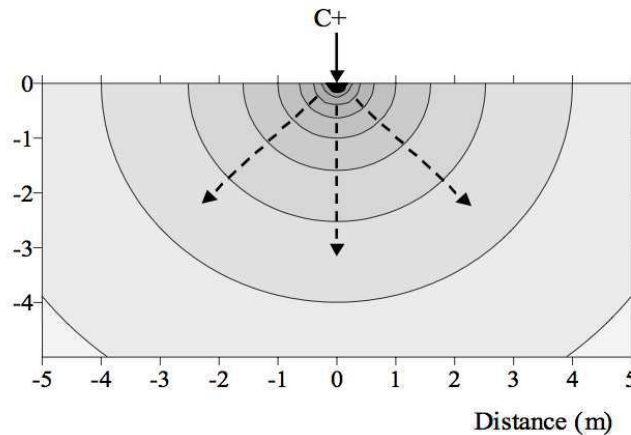
Fig 2: illustrates a 2-dimensional schematic depicting the injection of current into a homogeneous half space. The current electrode, denoted as C+, is featured in conjunction with C-, strategically positioned at an infinite distance. The figure portrays both the trajectories of current flow (illustrated by dotted lines) and the lines of equipotential (highlighted by bold lines). This visual representation is sourced from [Binley and Kemna, 2005].

This formulation allows to reconstruct the current potential distribution for any configuration and number of current electrodes inserted in a homogeneous medium.

In the practical application of the method, it is not possible to use a single point source, but at least 4 electrodes are positioned in the ground. A pair of electrodes, called energizers (AB), will serve to introduce the current, while through the second pair of electrodes (MN), the potential difference suffered by the signal along the path will be measured. Furthermore, the subsoil cannot be considered an ideal medium with homogeneous resistivity, in which the flow and current lines are distributed in an ideal manner.

In practice, then, to avoid the polarization effect of the electrodes, usually made of stainless steel, an alternating signal is used as current input. The shape of the current wave that represents this concept is the square wave (Fig 3).
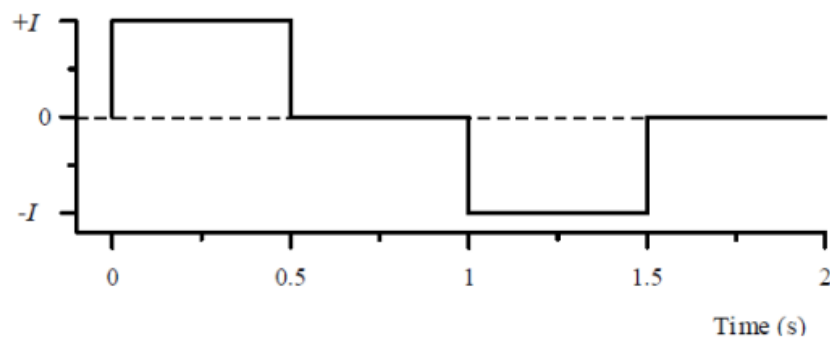
Fig 3: Shape of the square wave used in electrical resistivity investigations (Binley and Kemna, 2006).

The more generic electrode configuration is represented in Fig 4.
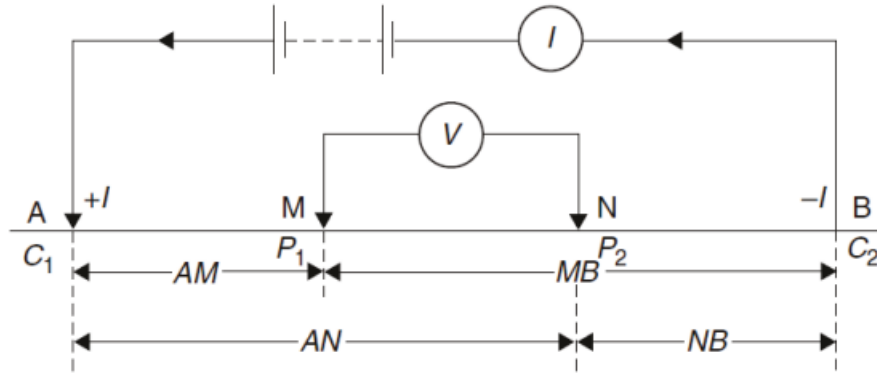
Fig 4: Common configuration of surface electrodes (Reynolds, 2011).

The potential difference measured between the electrodes M and N can be obtained as:

$$\Delta V_{MN} = \frac{I\rho}{2\pi}\left[\left(\frac{1}{AM} - \frac{1}{BM}\right) - \left(\frac{1}{AN} + \frac{1}{BN}\right)\right]$$

From which, setting k, called the geometric factor, specific for each electrode configuration, equal to:

$$k = \frac{2\pi}{\left(\frac{1}{AM} - \frac{1}{BM} - \frac{1}{AN} + \frac{1}{BN}\right)}$$

The formula for the apparent resistivity of the soil can be obtained, depending on the geometry of the layout and the values measured in the field of ΔV and I, according to the formula:

$$\rho_a = k\frac{\Delta V}{I} = kR$$

The apparent resistivity thus obtained is related to the configuration of the electrodes, it represents the resistivity that an electrically homogeneous and isotropic system should have to produce the same values of ⌊s and I. The real resistivity is obtained in the subsequent processing phases of the collected data. Through the inversion process it is also possible to obtain

thicknesses and resistivities of the various lithological horizons.

The evolution of the apparent resistivity is linked both to the resistivity and thicknesses of the different soil horizons. In the transition from a less to a more conductive horizon, the current will be distributed along well-spaced lines, within the more conductive ground. When moving to a more resistive layer, however, the current lines will tend to concentrate at the interface between the two layers, concentrating in the more conductive one.
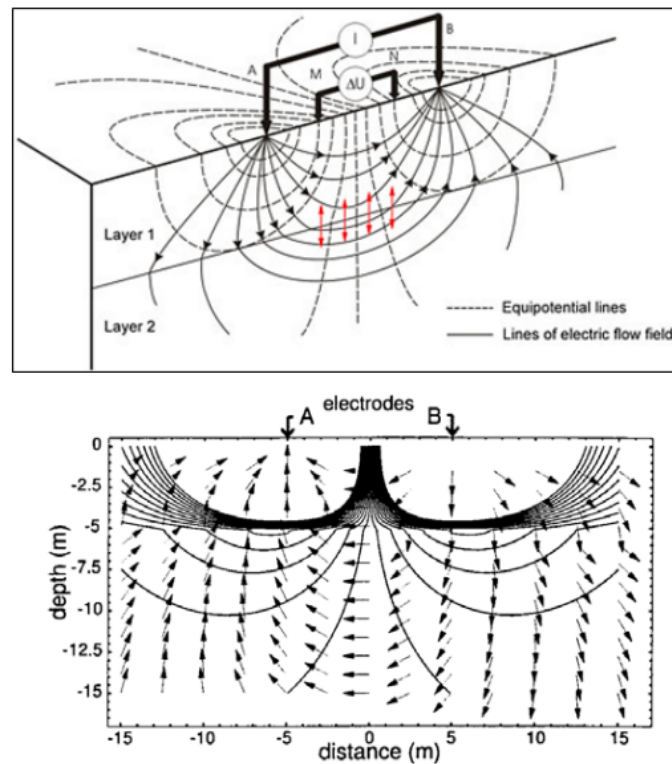
Fig 5: Distribution of current lines in the presence of layers with different conductivity.

2.2 Electrode arrays

It is possible to attribute different geometric configurations to the quadrupoles by varying the mutual position of the energizing and potentiometric electrodes. Each array has different resolution properties, both lateral and in relation to the depth of investigation. The mutual position of the electrode pairs influences the arrangement of the current lines in the investigated medium. The space between the current electrodes is characterized by a constant electric field.

The potential difference that develops is therefore a function of the distance between the potentiometric electrodes. It follows that the choice of the appropriate array must be made based on the objective of the measurement. The most common configuration is the Wenner, Schlumberger, Dipolo-Dipolo, multiple-gradient.

2.2.1 Wenner configuration

The Wenner array, a pivotal configuration in electrical resistivity imaging, employs four electrodes arranged in a linear sequence. Two outer electrodes inject current into the ground, while two inner electrodes measure the resulting potential difference. This arrangement fosters heightened sensitivity to vertical resistivity fluctuations, with the distance between potential electrodes standardized as 'a'. The geometric factor 'k', essential in calculating apparent resistivity, is derived as:

$$k = 2\pi a$$

This setup excels in yielding data with a notably high signal-to-noise ratio, ensuring more reliable measurements of subsurface resistivity changes. However, its predominant sensitivity to

vertical variations limits the resolution for detecting horizontal changes. Moreover, the investigative range is approximately half the spread's length, reflecting its capacity for discerning variations in resistivity along the vertical axis.

.
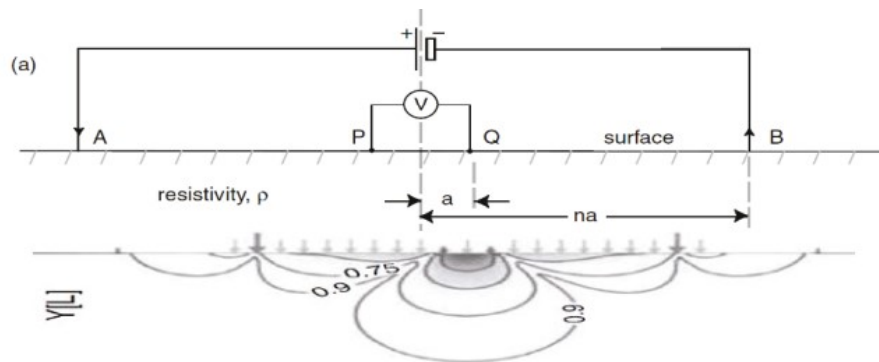
Fig 6: Configuration of the electrodes in the Wenner array and respective sensitivity (Everett, 2013).

2.2.2 Schlumberger Configuration

The Schlumberger array is another significant configuration used in electrical resistivity imaging. The potential electrodes are placed internally to the current electrodes. However, the distance between the potential electrodes is smaller than the distance between the current electrodes. The current electrodes are progressively moved apart according to multiples of 'a', while the potential electrodes remain relatively closer together.

The geometric factor 'k' in the Schlumberger array configuration is derived differently based on the arrangement of the electrodes and their distances. The geometric factor k is therefore equal to:

$$k = \pi \frac{AM\ AN}{MN}$$

The Schlumberger array is known for its sensitivity to horizontal resistivity variations. The

maximum sensitivity is achieved in the space between the potential electrodes, where the electrodes are closer together. Conversely, sensitivity is lower between the energizing (current) electrodes, where the spacing is larger. This setup allows for better detection and resolution of horizontal changes in resistivity compared to the Wenner array.

Unlike the Wenner array, the Schlumberger array tends to have a mediocre signal-to-noise ratio. This implies that the measured signal related to resistivity changes might be less pronounced compared to background noise, potentially requiring more sophisticated signal processing techniques for accurate data interpretation.
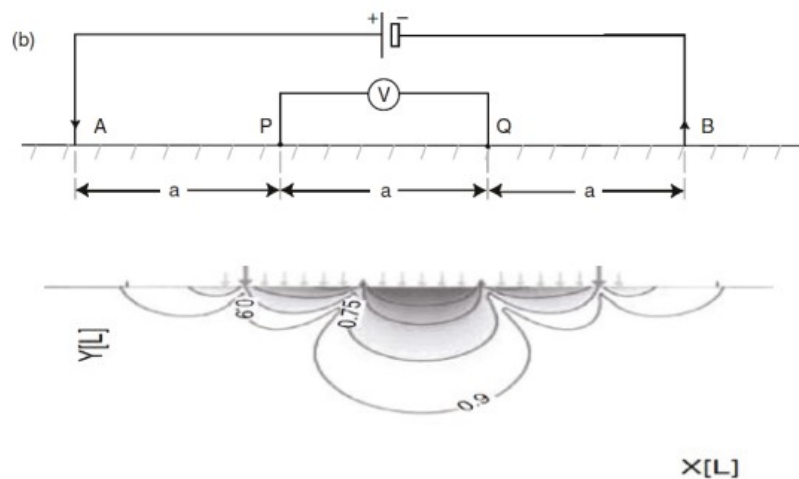
Fig 7: Configuration of the electrodes in the Schlumberger array and respective sensitivity (Everett, 2013).

2.2.3 Dipole-Dipole configuration

The Dipole-Dipole array is a significant configuration used in electrical resistivity imaging, comprising four electrodes placed in a linear sequence with a specific arrangement distinct from both the Wenner and Schlumberger arrays.

In this array, the potential electrodes are situated outside the current electrodes. Their

distance is precisely equal to an integer multiple of the distance between each pair of electrodes, maintaining a consistent separation throughout the array.

The geometric constant 'k' in the Dipole-Dipole array configuration depends on the specific arrangement of electrodes and their distances. The formula to determine 'k' is based on the geometry established by the electrode placement and their set distances from each other. The geometric constant is equal to:

$$k = 2\pi\, na\, (n+1)(n+2)$$

Maximum sensitivity in the Dipole-Dipole array is achieved beneath the two dipoles, where the electrodes are positioned. This array configuration excels in detecting horizontal resistivity variations due to its setup, but it tends to exhibit reduced sensitivity for vertical changes compared to the Wenner array.

The investigation depth achievable with the Dipole-Dipole array is approximately half the length of the spread. This indicates that its primary capacity lies in examining subsurface resistivity variations within a moderate depth range, and it might not penetrate as deeply as some other configurations.

The maximum sensitivity for this array occurs below the two dipoles. It is valid for horizontal resistivity variations, while it is reduced for vertical ones. The investigation depth that can be reached is approximately equal to half the length of the spread.
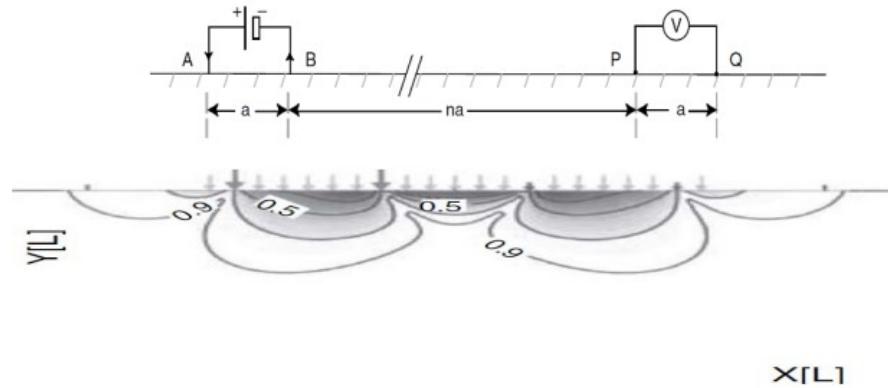
Fig 8: Configuration of the electrodes in the Dipole-Dipole array and respective sensitivity (Everett, 2013)

2.2.4 Multiple-gradient configuration

Multi-electrode gradient surveying involves the injection of electrical current with a specific separation distance of (s+2)a, as shown in Figure 1. Simultaneously or sequentially, potential differences are measured between the potential electrodes, which have a spacing of a. The separation factor 's' is an integer representing the maximum number of potential readings achievable for a single current injection.

The factor 'n' characterizes the relative spacing between the potential dipole and the nearest current electrode.
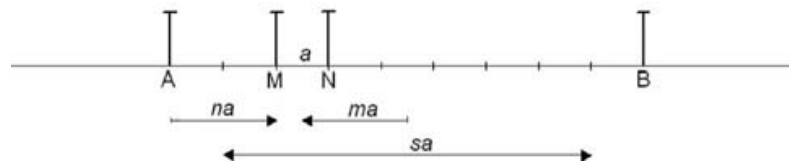
Fig 9: there is a diagram illustrating a multiple-gradient array, highlighting the electrode positions for a measurement conducted with a separation between current electrodes of (s+2)a, where the separation factor 's' equals 7. The 'n-factor' is set to 2, which is defined as the smallest relative spacing between a current electrode and a potential electrode. Additionally, the 'midpoint factor' 'm' is given as -2.

To further characterize the surveying setup, a midpoint factor 'm' can be defined. This 'm' factor

25

represents the position of the midpoint of the potential electrode dipole relative to the midpoint between the two current electrodes. This allows for a more precise description of the spatial arrangement and measurements in the surveying process.

$$m = \frac{\frac{(x_M + x_N)}{2} - \frac{(x_A + x_B)}{2}}{(x_N - x_M)} = \frac{x_{MN} - x_{AB}}{a}$$

The positions of the current and potential electrodes are denoted as x_A, x_B, x_M, and x_N, with the condition that $x_B > x_A$ and $x_N > x_M$. Additionally, x_{AB} and x_{MN} represent the midpoints of the respective dipole setups.

To explain further, a negative m-factor signifies that the potential dipole is positioned to the left of the current electrode midpoint, while a positive m-factor indicates that the potential electrode dipole is shifted to the right in relation to the midpoint.

For data processing convenience, it may also be useful to define the n-factor as a vector. In this definition, positive n-factors would indicate that the potential electrodes are at higher coordinates than the nearest current electrode, and negative n-factors would indicate that they are at lower coordinates. It follows that, for given s and n values, m is also determined as:

$m = n - \frac{s+1}{2}$ for $x_{MN} \leq x_{AB}$ (m ≤0),

And

$m = n + \frac{s+1}{2}$ for $x_{MN} > x_{AB}$ (m >0),

where n and m are negative or positive integers.

2.3 Processing and inversion of geophysical data

The main objective of the application of electrical methods is to obtain and model the spatial distribution of electrical resistivity in the subsoil, starting from a series of measurements conducted on the surface and based on Ohm's law. This result is achieved by subjecting the data collected in the field to an inversion procedure. In the iterative nonlinear regression phase (the relationship between the apparent resistivity and the model parameters is nonlinear), the measured data are compared with those simulated by the direct model, to arrive at a final model that minimizes their differences.

The raw data measured by the geo-resistivimeter can be represented graphically with a pseudosection of apparent resistivity. The inversion process allows the pseudo-resistivity to be transformed into real resistivity of the ground. The estimate of the model parameters must be as consistent as possible with the observed data. However, the inversion procedure is not able to provide a unique result, due to the presence of instrumental errors and incompleteness in the field data which are always present in the dataset.

2.3.1 Determination of the error

It is important, as a preliminary phase of data processing, to estimate the error existing in the starting dataset. We proceed for this purpose by carrying out the control of direct and reciprocal measurements. Theoretically, the reciprocal measurement should provide the same resistivity value as the corresponding direct measurement, according to the principle of reciprocity. In reality, two different results are obtained, because each measurement is subject to error. This approach therefore allows us to obtain a conservative estimate of the quality of the

campaign dataset.

It is essential to take into account the intrinsic error of the measurements, because the final reconstruction of the resistivity image is strongly affected by the quality of the starting data. A poor quality dataset generates a model that is not very representative of reality. Mutual measurements are essential to avoid using data affected by errors higher than a certain established threshold. The intrinsic error of the data can derive from:

• poor contact between the electrode and the ground,

• random errors deriving from instrumentation,

• external factors

2.3.2 Forward model

The forward model calculates the resistances that would theoretically be obtained for a certain resistivity distribution. It is therefore a simulation model of reality. It is based on the equation of steady flow of direct current in a heterogeneous and anisotropic medium, which is described by the differential equation:

$$\frac{d}{dx}\left(\sigma_x \frac{dV}{dx}\right) + \frac{d}{dy}\left(\sigma_y \frac{dV}{dy}\right) + \frac{d}{dz}\left(\sigma_z \frac{dV}{dz}\right) = 0$$

expressed in compact form as:

$$\nabla \cdot (\sigma \nabla V) = 0$$

which allows, for a certain distribution of electrical conductivity, to obtain the electrical potentials, respecting the appropriate boundary conditions. In solving complex 2D or 3D cases,

finite difference and finite element numerical methods are commonly applied. The space is discretized into cells, to each of which a conductivity value is assigned, while the potential is calculated at the nodes of the various cells, in correspondence with which the electrodes are positioned. The discretization of the space is denser near the electrodes, where the sensitivity of the measurement is greater, and is reduced as you move away from it.

2.3.3 Inverse model

The data inversion phase, i.e. the conversion of the apparent resistivity values into real resistivity, is determined by resolving the inverse model, which calculates the resistivity distribution as a function of the acquired measurements. We proceed by dividing the space into cells, characterized by their own conductivity value σ. The distribution of conductivity in the space thus discretized is represented by a vector m_j:

$$m_j = ln\sigma_j \ (j = 1, \dots, M)$$

in which conductivity appears in logarithmic form, due to the vast range of values that it can acquire. The solution of the inverse model is composed of the best set of parameters m_j which represents the experimental data d of the resistance obtained from the direct model, respecting the imposed uncertainty threshold.

This result is obtained by solving an objective function $\psi_d(m)$ to be minimized, in which the measured resistance values d and calculated with the direct model 'f(m)' are present:

$$\Psi_d\,(m) = \ \|W_d\,[d - \ f(m)\|^{\,2}$$

However, due to the intrinsic non-uniqueness of the resistivity in the solution of the

inverse problem, together with the presence of the error in the data, the use of the data misfit alone can lead to an extremely ill-posed numerical problem. Consequently, additional constraints must be imposed on the

inversion. This is commonly done by introducing a stabilization function for the model $\psi(m)$ into the objective function. The objective function will at this point be described by the formula:

$$\Psi(m) = \Psi_d(m) + \alpha\,\Psi_m(m)$$

in which there are the objective function referring to the misfit of the data ψ_d, the function referring to the model ψ_m, between the misfit and the objective function of the inversion model. (Binley and Kemna 2005) These operations are performed by software that proceeds automatically, after the operator has provided them with the minimum information useful for the inversion. In this work, the ResIPy software was used, an inverse modeling program that can be used for 2D electrical resistivity distributions, based on the three-dimensional computation of current flows on a square finite element mesh.

2.4 Regularization Techniques in Geophysical Inversion

Geophysical inversion endeavors to derive a reliable model of subsurface properties by interpreting observed data. However, the inherent ill-posed nature of this inverse problem introduces challenges due to its susceptibility to multiple equally plausible solutions and sensitivity to data noise. Regularization techniques serve as indispensable tools to address these issues, enhancing the stability, reliability, and physical realism of the obtained models.

- Tikhonov Regularization

Tikhonov regularization stands as a fundamental technique in geophysical inversion. It involves

introducing a penalty term into the inversion process, aiming to balance the fidelity to observed data with the desired model characteristics. This penalty term minimizes the model's roughness or complexity, ensuring a smoother and more geologically plausible outcome. The regularization parameter plays a pivotal role in governing the trade-off between data fit and model smoothness.

- Smoothness Constraints

Smoothness constraints serve as an additional mechanism to regulate the inversion process, primarily targeting the prevention of sharp discontinuities or artifacts within the subsurface model. Particularly valuable when dealing with noisy data, these constraints promote the generation of more continuous and coherent subsurface representations, aligning with geological expectations.

- Joint Inversion

Another influential regularization strategy involves the integration of diverse geophysical data types, such as seismic and electrical resistivity data, through joint inversion techniques. This approach leverages multiple datasets to enhance the robustness of the inversion process and constrain the resulting model. By combining different types of information, joint inversion facilitates a more comprehensive understanding of subsurface structures, improving model reliability.

These regularization techniques collectively aim to enhance the stability, uniqueness, and physical realism of inversion results. By incorporating additional information or assumptions about the subsurface into the mathematical formulation of the inversion process, regularization significantly mitigates the ill-posed nature of the problem. Ultimately, it fosters more reliable and geologically plausible interpretations of subsurface properties, crucial for various geophysical

exploration and characterization endeavors.

3.0 ResIPy sofware

ResIPy is a Python-based, open-source software designed to streamline the processing, modeling, and inversion of geoelectrical data. Its primary focus is on 2D applications, providing an intuitive interface for users in educational and training environments. The software employs inverse methods to translate geoelectrical measurements into resistivity distributions, aiming to minimize the misfit between observed measurements and predicted responses from a geoelectrical model.

One key aspect of ResIPy is its commitment to accessibility, addressing the challenges associated with non-commercial tools that often require substantial expertise to operate effectively. The software is tailored to be user-friendly, with a graphical user interface (GUI) that eliminates the need for command-line operations. This design choice enhances its suitability for educational purposes, enabling new users to explore geoelectrical data analysis at their own pace.

The core functionality of ResIPy includes importing, filtering, and error modeling of geoelectrical data. The software utilizes the R2, cR2, and R3t codes for modeling and inversion, which are established tools in the field of resistivity problems. These codes, while powerful, lack a graphical user interface, and ResIPy bridges this gap by providing an intuitive GUI for users.

ResIPy's capabilities extend to 3D applications, as documented in Boyd et al. (2019), although this aspect will not be detailed in this 2D-focused manuscript. The software supports complex mesh construction using the Gmsh meshing code, allowing flexibility in electrode assignment and accommodating various survey configurations, including surface and borehole electrode-based surveys.

The software's philosophy revolves around maintaining the sophistication required for geoelectrical inversion while enhancing accessibility for a broader user base. Its open-source nature encourages contributions from users and developers, fostering a collaborative environment in the scientific community. Additionally, ResIPy serves as a valuable tool for reproducible science, allowing users to customize the code to suit their specific needs.

ResIPy's architecture is organized into three distinct layers, each playing a crucial role in the software's functionality.

- Bottom Layer: Compiled Inversion Codes and Meshing Software

This foundational layer encompasses compiled inversion codes, specifically R2, R3t, and cR2, along with meshing software like Gmsh. These inversion codes are responsible for executing the core processes of inversion and forward modeling for DC resistivity and complex resistivity. Gmsh, a meshing tool, contributes to the construction of triangular meshes, providing a crucial element for accurate geoelectrical modeling.

- Middle Layer: Python API as a Wrapper

The middle layer serves as a bridge between the bottom layer's compiled codes and the user interface. This layer is built around the Python API, which acts as a wrapper around the executable codes. This design simplifies the interaction with the underlying codes, making it more accessible for users. The Python API facilitates the creation of input files, such as R2.in and mesh.geo, and manages the output files, enhancing the user experience during the geoelectrical data processing and inversion.

- Top Layer: Visualization Tools for User Interaction

The top layer focuses on providing users with a graphical interface and visualization tools. It encompasses features that enable users to interact with the software intuitively. Visualization tools within this layer offer a graphical environment where users can observe and interpret geoelectrical data, inversion results, and other relevant information. This layer enhances the overall user experience, making ResIPy more user-friendly and accessible.

- Documentation Following scipy/numpy Docstring Guidelines

ResIPy's documentation adheres to the guidelines set by the scientific computing libraries scipy and numpy for docstring formatting. This ensures that the documentation is clear, well-organized, and easily understandable for users. Following these guidelines is crucial for providing comprehensive information about ResIPy's functionalities, parameters, and usage, aiding users in effectively utilizing the software for geoelectrical data analysis.

3.1 Standalone Graphical User Interface (GUI):

ResIPy features a standalone graphical user interface (GUI) designed using PyQt5, ensuring flexibility for modifications and accommodating future developments. The GUI simplifies user interactions and incorporates functionalities for visualizing and exporting data using matplotlib (Hunter, 2007). The design is tab-based, providing a non-linear workflow to guide users through essential stages of data processing, mesh generation, and inversion.

- Tab-Based Workflow (Fig. 3)

The GUI comprises a series of tabs that enable a non-linear workflow. These tabs guide users through various stages, including importing and filtering data, generating a mesh, and performing inversions.
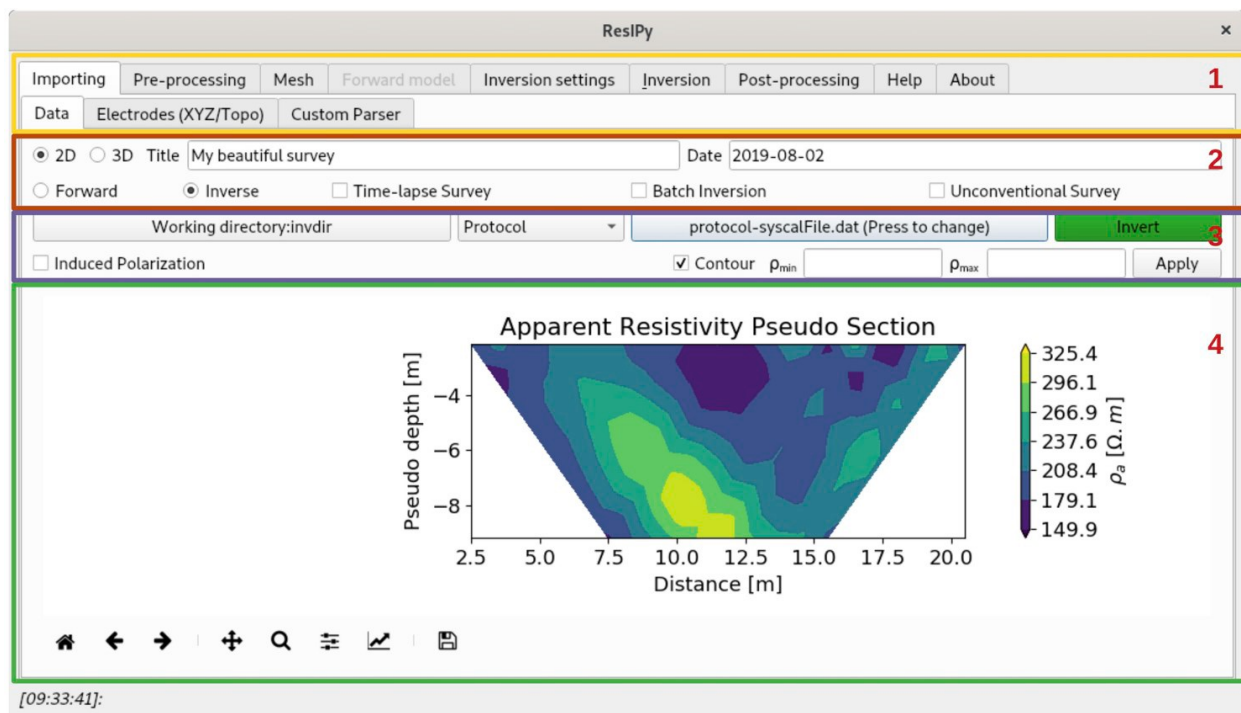

Fig 10: illustrates the overall structure of the independent graphical user interface, featuring:(1) Multiple tabs designated for distinct processing stages, (2) Selection options for survey type and

inverse/forward modeling, (3) Functions for data import and IP verification, (4) A graphical representation displaying pseudo-section plots of the imported data.

- Import Tab

The "Import" tab serves as the starting point for loading geoelectrical and topographical data. Geoelectrical data can be directly imported in standard formats (e.g., IRIS Instruments Syscal files, Res2DInv files, R2, and cR2 input files). Alternatively, users can employ the "Custom Parser" tab for manual import. Topographical data, essential for accurate modeling, can be entered manually or loaded from a comma-separated value (csv) file at the "Electrode (XYZ/Topo)" tab.

- Workflow Flexibility

Following data import, users can progress through the workflow or directly initiate inversion using default settings with the "Invert" button in the "Importing" tab. Default settings are optimized for reliability in most cases, providing a convenient option for novice users or quick data assessments in the field.

- Inversion Settings

All inversion parameters available in R2 and cR2 are accessible and modifiable under the "Inversion settings" tab. Users can adjust parameters such as regularization type, conversion of data to logarithmic values, data error estimates, smoothing anisotropy, and the maximum number of iterations. Help is available for each parameter, and additional details can be found in the R2 and cR2 manuals (http://www.es.lancs.ac.uk/people/amb/Freeware/Freeware.htm).

- Advanced Settings

Under advanced settings, users have the option to perform batch inversions in parallel on multicore machines. This feature enhances efficiency, allowing simultaneous processing of multiple inversions, particularly useful for large datasets and advanced users seeking optimization.

3.2 Data quality control

ResIPy offers robust data cleaning and quality control capabilities, providing users with the flexibility to perform these tasks automatically or with manual intervention. The approach chosen considers the presence of reciprocal measurements in the dataset, enhancing the reliability of the quality control process. In the graphical user interface (GUI), users can access data quality control options conveniently located under the "Pre-processing" tab. This tab serves as a dedicated space for managing and enhancing the quality of geoelectrical data before proceeding with subsequent processing steps.

3.2.1 Automatic data cleaning/filtering

Automatic data cleaning and filtering in ResIPy involves the initial application of the *basicFilter()* method, which systematically eliminates specific types of measurements to enhance data quality. This method is designed to remove the following categories of measurements:

- Infinity or NaN Values

The *basicFilter()* method identifies and eliminates measurements containing infinity or NaN (Not

a Number) values, ensuring the dataset is free from such inconsistencies.

- Duplicates

Duplicate measurements are automatically detected and removed. This step helps maintain data integrity by eliminating redundant information.

- Invalid Measurements

The method targets invalid measurements, specifically those where quadrupoles have current electrodes also serving as potential electrodes (A or B at the same position as M or N). ResIPy ensures the integrity of the dataset by excluding such invalid measurements.

If the dataset includes reciprocal measurements, ResIPy further engages the *computeReciprocal()* method, calculating reciprocal errors. The software automatically identifies measurements with a relative reciprocal error exceeding 20%, notifying the user through the API. It's important to note that, by default, ResIPy does not discard measurements with high reciprocal errors, providing transparency to the user.

Moreover, these data cleaning methods, including *basicFilter()* and *computeReciprocal()*, are also invoked when a dataset is manually added using the *addData()* function. This scenario may occur when a reciprocal dataset is added separately, ensuring that consistent data cleaning procedures are applied regardless of how the data is incorporated into ResIPy.

3.2.2 User-Controlled Quality Control Methods in ResIPy

In addition to the automatic data cleaning step, ResIPy provides users with various user-controlled quality control methods available through both the code API and the graphical user

interface (GUI). These methods are categorized into two groups: (1) data cleaning/filtering and (2) data error analysis.

Data Cleaning/Filtering:

User-controlled data cleaning and filtering are conducted through multiple distinct steps, all accessible in the GUI under the "Pre-processing" tab. When dealing with datasets containing reciprocal measurements, users have the following options within the "Reciprocal Filtering" tab under "Pre-processing":

- filterRecip(percent):

This method allows users to specify a desired percentage value ('percent') to remove measurements with high error.

- removeUnpaired():

Removes quadrupoles that lack a reciprocal pair. These methods are presented in an intuitive interface along with an error probability distribution histogram (Fig. 4c) to aid users in visualizing dataset quality.

Additionally, users can selectively remove unwanted measurements, irrespective of reciprocity, using the filterManual() method. This interactive method is available in the GUI under the "Manual/Reciprocal Filtering" tab within "Pre-processing." It enables users to manually select and remove data points directly within the GUI. Moreover, users can eliminate all measurements associated with a specific electrode, as depicted in Fig. 4a and b.
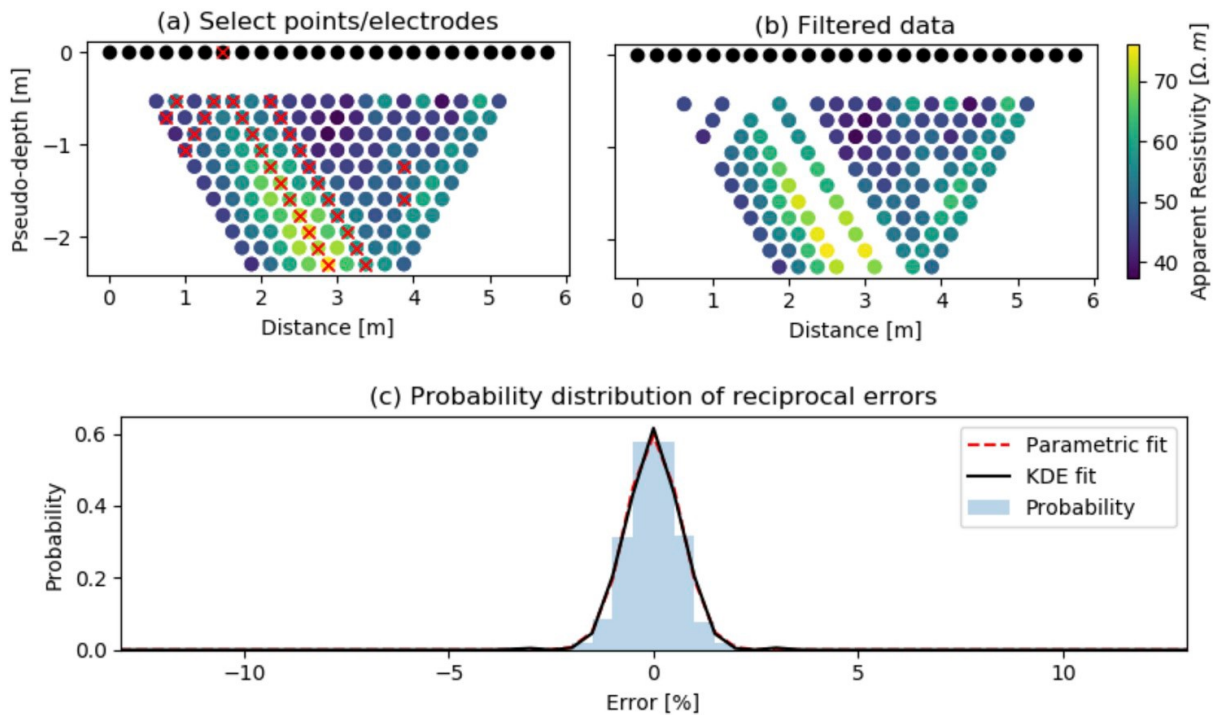
Fig 11: Interactive Manual Filtering. This figure illustrates the interactive manual filtering process, allowing users to visually identify and select unwanted data points in the pseudo section. Subsequently, the removal of these selected data points is facilitated by pressing the "Apply" button. The probability distribution of reciprocal errors, presented with parametric and non-parametric fits, enhances the understanding of dataset quality. (a) Pseudo Section with Selected Unwanted Data Points: Displaying a pseudo section where undesirable data points are highlighted and crossed out in red. (b) Pseudo Section with Removed Data Points: Presenting the pseudo section after the removal of the selected data points. To execute the removal, the user needs to press the "Apply" button. (c) Probability Distribution of Reciprocal Error: Depicting the probability distribution of reciprocal errors with both parametric and non-parametric fit, utilizing Kernel Density Estimate (KDE).

Further user-controlled data cleaning/filtering is directed towards datasets with chargeability/phase values, accessible through the "Phase Filtering" tab in "Pre-processing." Quality control measures become particularly crucial for IP applications due to the smaller signal-to-noise ratio compared to DC resistivity problems (Slater and Lesmes, 2002; Zarif et al., 2017).

Data Error Analysis

ResIPy goes beyond data cleaning by offering sophisticated data error modeling capabilities for DC resistivity. The GUI includes dedicated tabs for data error analysis, namely the "Resistance Error Model". It's important to note that these tabs become active only when reciprocal measurements are present within the input datasets.

- Resistance Error Model

The observed errors in resistance (R_{error}) are determined by individual measurement reciprocal errors, expressed as:

$$R_{error} = |R_{normal} - R_{reciprocal}|$$

To establish an error model, whether linear or power-law, ResIPy employs multibin analysis. This methodology, detailed in Koestel et al. (2008) and Mwakanyamale et al. (2012), involves binning errors into 20 bins of equal count. The sorting is then based on the average resistance error (R_{avg}) [Ω], computed as:

$$R_{avg} = \left| \frac{R_{normal} + R_{reciprocal}}{2} \right|$$

This systematic approach to error analysis enhances the accuracy of error modeling and provides users with valuable insights into the reliability of resistance data.

3.3 Meshing in ResIPy

In ResIPy, the meshing process involves the utilization of two types of 2D finite element meshes: structured quadrilateral meshes and unstructured triangular meshes. Regardless of the elemental shape chosen, the mesh design ensures that elements are finer near the electrodes and gradually become coarser at greater distances from the electrodes. This strategic mesh refinement aims to address the necessity for higher discretization in regions characterized by a high potential multiple-gradient.

The mesh structure consists of a finer mesh defined by the electrode locations, enveloped within a coarser mesh with larger lateral and depth extents, especially applicable for semi-infinite boundary problems. The non-flux (Neumann) nature of the mesh boundaries requires them to be sufficiently far away from electrode positions to reliably model electrical current flow, as R2 and cR2 simulate current flow for the entire assigned mesh.

In typical field scenarios, electrical current from the electrodes extends beyond the survey boundaries. To accommodate this, the ResIPy mesh includes a fine mesh region whose lateral extent is determined by the X (horizontal) coordinates of electrodes, represented as nodes in the mesh. The depth of this fine mesh region is estimated using the formula:

$$Z_{min} - \frac{2X_{max}}{3}$$

Where Z_{min} is the lowest elevation of electrodes in the surface or borehole array, and X_{max} is the distance between the longest quadrupole in the survey.

It's essential to note that this depth estimate ($Z_{min} - \frac{2X_{max}}{3}$) is not a depth of investigation, as calculated by methods such as Oldenburg and Li (1999). Instead, it serves as a conservative

estimate to facilitate the meshing process. There are exceptions, such as when conducting electrical surveys near cliff faces or in laboratory tank experiments, where infinite boundaries may not be suitable. In such cases, ResIPy allows the import of custom meshes tailored to specific requirements.

- Quadrilateral Mesh

In ResIPy, a quadrilateral mesh is defined as an array of X and Z coordinates, forming a structured grid. This grid structure is essentially a fine region defined by the survey geometry, surrounded by a coarser region due to the imposition of infinite boundaries. It's important to note that, in the ResIPy graphical user interface (GUI), only the finer mesh region is displayed.

Adjustments to the number of nodes between electrodes can be made in the GUI to enhance the control over mesh refinement. Additionally, in the API, users have the flexibility to modify mesh growth factors in the Z direction using attributes such as **zf** and **zgf** for the fine and coarse regions, respectively. For the X direction, a growth factor for the coarse region can also be set through the API using the **xgf** attribute.

In scenarios involving buried electrodes, such as cross-borehole surveys, the X and Z coordinates of these electrodes are inserted into the quadrilateral mesh after the primary mesh generation scheme. This ensures that the mesh accurately represents the survey geometry, accounting for the specific arrangement of electrodes and allowing for precise modeling of subsurface electrical properties.

- Triangular Mesh in ResIPy

Triangular meshes in ResIPy offer increased versatility, enabling application to more complex geometries such as topography and intricate features within the study area. The mesh generation process is facilitated by the **trian_mesh()** function in ResIPy, which calls Gmsh.exe to perform the meshing operation. This function involves creating an input file for Gmsh (.geo) and parsing the output file (.msh).

Similar to the quadrilateral mesh, users can control mesh refinement by specifying a characteristic length associated with each electrode node. Smaller characteristic lengths result in a finer mesh. Additionally, a growth factor can be specified to control the increase in element size with depth. Both of these parameters can be adjusted in the GUI using sliders or in the API through the **cl_factor** and **gf** attributes of the **R2.createMesh()** method.

It is advisable to avoid fine elements in areas with low sensitivity, as they contribute minimally to the interpretation of the inverted model while increasing computation time. Both quadrilateral and triangular mesh options are available in ResIPy, catering to the capabilities of the R2/cR2 codes. While a quadrilateral mesh is generated faster and is easier to work with for certain tasks (e.g., extracting vertical or horizontal resistivity profiles), triangular meshes are more versatile. They can account for complex topography and offer computational efficiency. As a result, ResIPy recommends the use of triangular meshes for enhanced modeling and interpretation capabilities.

- Whole Space Problems

In specific scenarios, it may be suitable to assume that electrodes are buried at such extensive

depths that the current flow does not interact with the surface or any other boundaries. ResIPy accommodates such cases by providing a scheme where electrode coordinates are incorporated into a fine triangular mesh region surrounded by a larger region.

This approach in ResIPy is designed for situations where the influence of current flow does not extend beyond the electrode positions, effectively treating the problem as a "whole space" scenario. The electrode coordinates are inserted into a finer mesh region within the triangular mesh, and this fine region is enveloped by a coarser surrounding mesh. The larger region ensures that the mesh boundaries are sufficiently far away from the electrode positions, considering the non-flux (Neumann) nature of the boundaries.

This methodology is particularly applicable when dealing with extensive burial depths, where the current from electrodes is assumed not to propagate beyond the survey bounds. It is essential for accurately modeling current flow in scenarios where infinite boundaries are not suitable, such as when conducting electrical surveys near cliff faces or in laboratory tank experiments. ResIPy's flexibility in handling such whole space problems enhances its applicability to diverse geophysical scenarios.

3.4 Region Definition

In ResIPy, users have the capability to define different regions within the mesh, serving the purpose of generating forward models for survey design or conducting inverse modeling with known subsurface boundaries. These regions allow users to assign specific resistivity values, offering a valuable tool for simulating and analyzing geoelectrical scenarios.

The definition of regions in ResIPy is facilitated through an interactive process in the graphical

user interface (GUI). Users can select and delineate regions using an interactive plot picker and table system, as illustrated in Fig. 8. Each region can be assigned unique resistivity values, enabling a detailed specification of subsurface properties in the model.
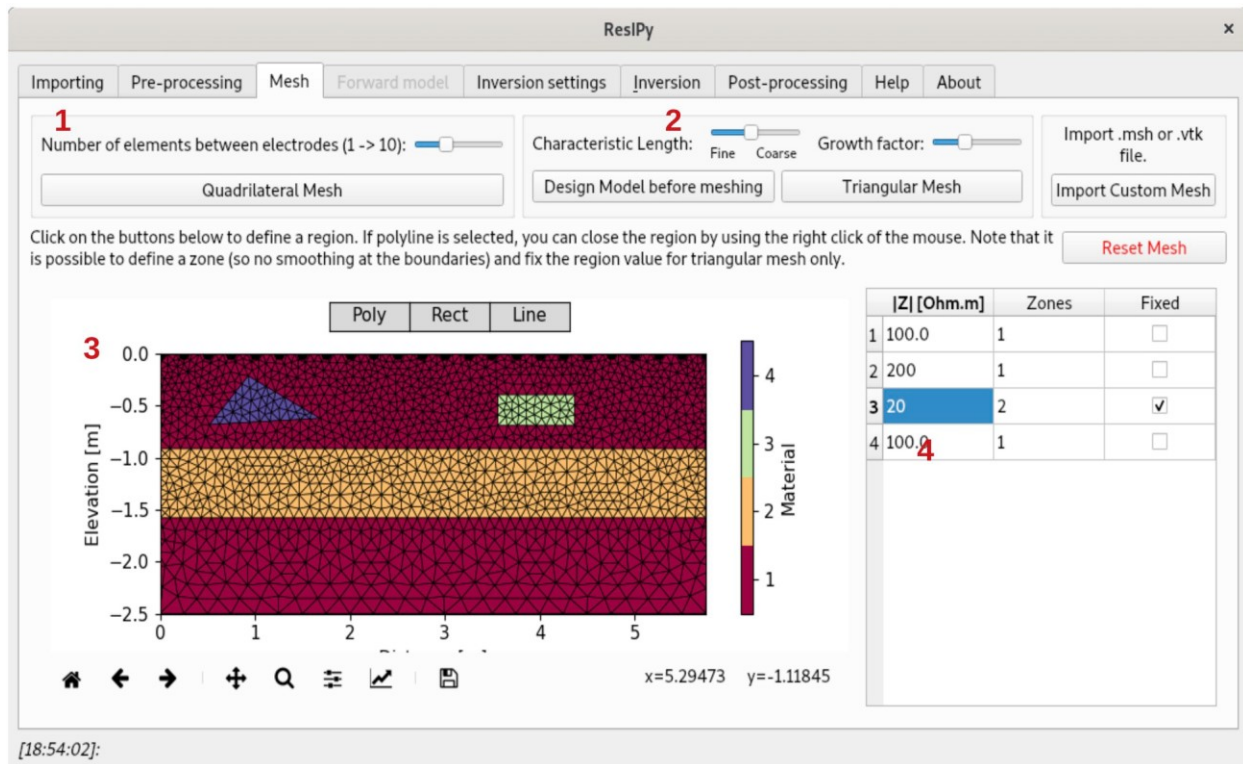

Fig 12: illustrates the user-friendly interface in ResIPy for both quadrilateral (1) and triangular (2) mesh generation. The interactive mesh display offers a versatile platform for drawing regions of various shapes (3), enhancing the flexibility of defining spatial elements. Users can conveniently specify the properties of these regions using the panel on the right (4), ensuring a seamless and intuitive experience.

In certain cases, users may want to influence the inversion process by preventing regularization across specific boundaries. This is particularly relevant when there are known geological boundaries that should be treated as distinct zones. ResIPy provides the functionality to specify these regions as different zones, where regularization is suppressed along their boundaries.

It is crucial to note the distinction between the terms 'region' and 'zone' in ResIPy. A 'region'

refers to a spatial group of elements defined by the user, while a 'zone' is a specific case of a

region where regularization is intentionally suppressed along its boundaries. This clear

differentiation enhances the flexibility and precision of modeling and inversion processes.

3.5 Parameterization

In the context of a forward model calculation, it is essential to define the resistivity for each element. In contrast, for an inverse solution, the starting resistivity model is typically a uniform model. When operating in inverse mode, it becomes crucial to set the discretization of parameters. The simplest approach involves treating each finite element as a separate parameter. However, in certain scenarios, a more intricate parameterization may be necessary.
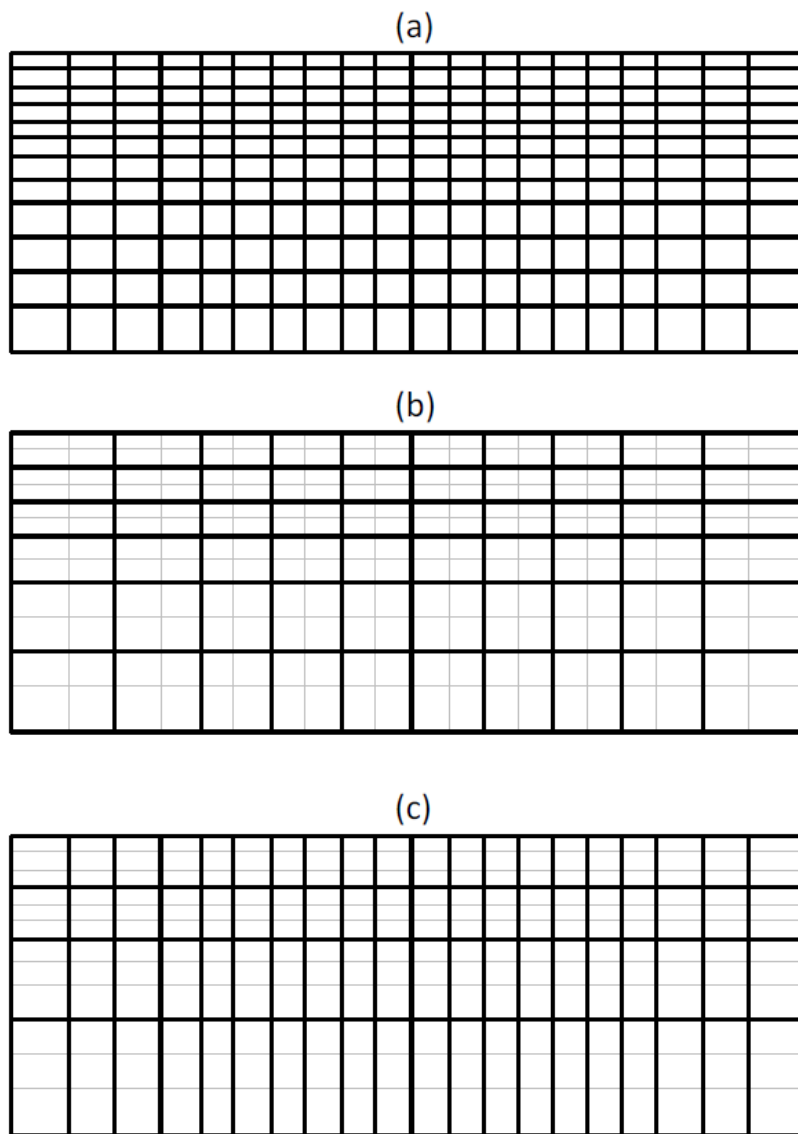
(a)

(b)

(c)

Fig 13: illustrates the delineation of parameter boundaries within a structured mesh. The finite

element mesh is depicted in grey lines, while the black lines demarcate the parameter zones. In (a), each individual element serves as a parameter. In (b), parameters are configured as 2 x 2 patches of elements. Finally, in (c), parameters are organized as 3 x 1 patches of elements.

In a structured quadrilateral mesh, ResIPy introduces the concept of 'patch' sizes for parameters, as illustrated in Figure 13. A patch, in this context, refers to a group of elements. The strategic grouping of elements into patches offers the advantage of reduced computational time, as it effectively decreases the total number of parameters. This streamlined parameterization process contributes to the efficiency of the inversion process.

There are situations where it is desirable to set the resistivity to a fixed value within a specific portion of the mesh. In other words, parameters should only be active in a subset of the finite element mesh, as depicted in Figure 14. R2 facilitates this kind of parameterization by specifying the starting and ending points of patching in both the x and y directions. This functionality allows users to selectively control which parts of the mesh undergo parameter adjustments, providing a flexible approach to resistivity modeling in specific regions.
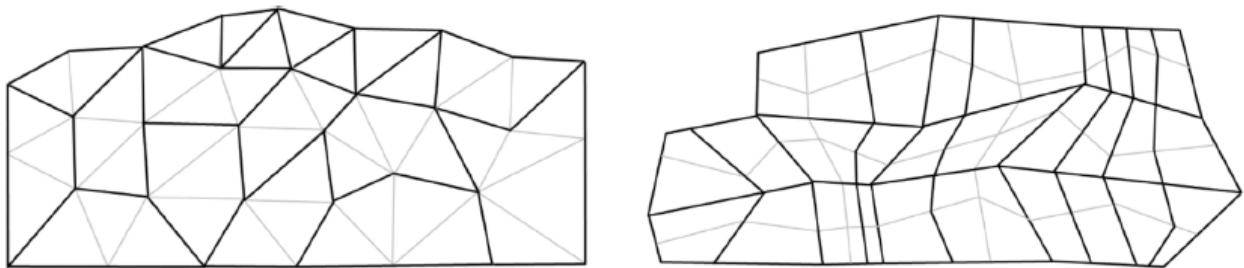

Fig 14: depicts the parameterization of a specific subset within the structured finite element mesh. The grey lines represent the finite element mesh, while the black lines outline the designated parameter zones.

For a more detailed and customized control over parameterization, users can take advantage of a pre-prepared mesh, whether it's a triangular or quadrilateral mesh (as illustrated

in Figure 14). This involves assigning a specific parameter number to each element in the mesh.dat file. Notably, if an element is assigned a parameter number of 0, the inverse solution will automatically fix the resistivity of that particular element to its initial value. This advanced parameterization approach offers users greater precision and flexibility in tailoring the resistivity model to specific elements within the mesh.
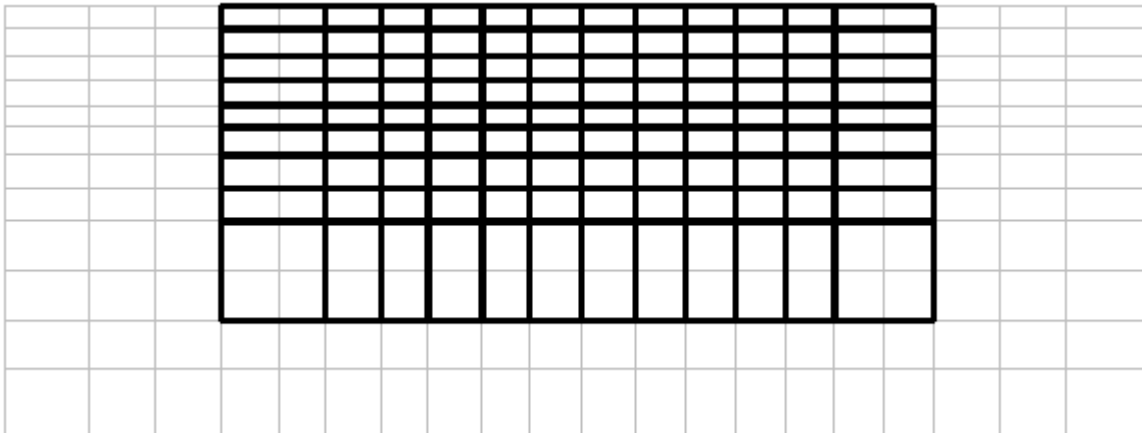

Fig 15: illustrates the parameterization of an unstructured mesh as defined in mesh.dat. The grey lines represent the finite element mesh, and the black lines indicate the boundaries of the designated parameters.

Enhanced control over parameterization is accomplished by implementing 'zoning' of parameters in R2. A zone is characterized as a consistent grouping of parameters, as illustrated in Figure 16. Importantly, smoothing in the inverse solution does not extend across zones. This feature proves beneficial when a priori information enables the user to delineate sharp contrasts, such as at a water table boundary.

Figure 16 depicts the zoning of parameterization, where distinct colors signify different parameter zones within the mesh. Once again, complete flexibility is achievable with an unstructured mesh.
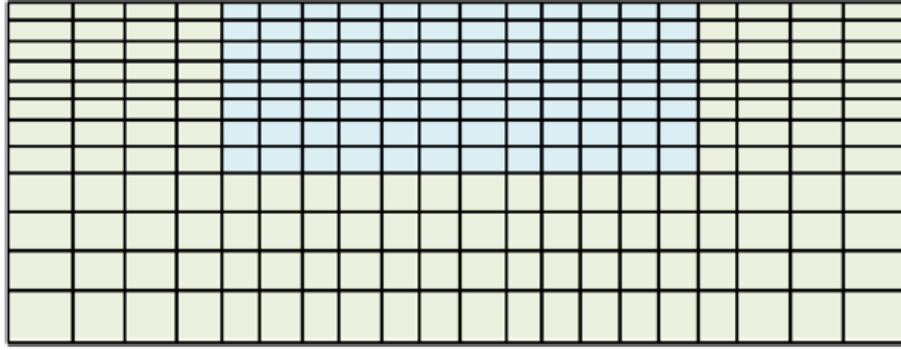
Fig 16: The mesh.dat file defines the parameter and zone for each element, providing comprehensive control over the parameterization process.
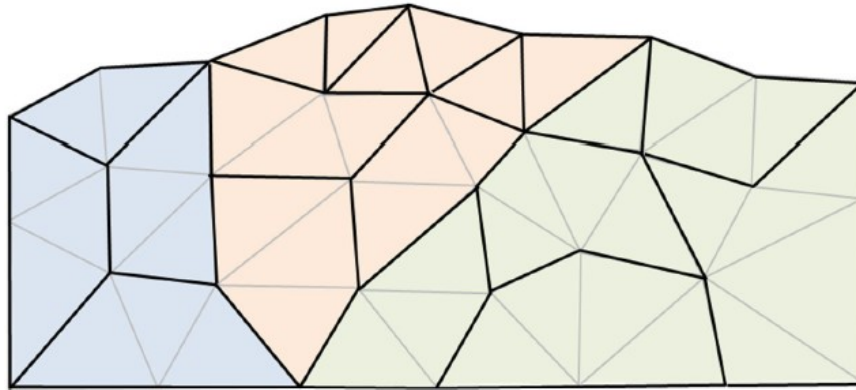

Fig 17: displays zoning for parameterization in an unstructured triangular mesh, with distinct colors representing different parameter zones.

To summarize, when defining a mesh in mesh.dat, each element is allocated (i) a parameter number (which is set to zero if it should remain fixed during the inversion); and (ii) a zone number. In the majority of cases, the parameter number corresponds to the element number, and the zone is designated as 1.

4.0 Results and Discussion

4.1 Site description

The experiment was conducted at the Experimental Farm "L. Toniolo" of the University of Padova in Legnaro (45°21' N; 11°57' E, 8 m a.s.l.), North-Eastern Italy. In the study area, the soil is classified as Fluvi- Calcaric Cambisol (WRB, 2014) and represents almost 50% of the Venetian plain in the Veneto region. It is a poorly layered silt-loam soil with low natural fertility due to little soil organic carbon content (about 8-10 g kg-1 at the 0-20 cm layer, down to 0.5 g kg-1 at 60-90 cm) and low cation exchange capacity (< 20 cmol kg-1)(Longo et al., 2021).

4.2 Electrical resistivity instrument and Data acquisition

The Syscal Terra is the new generation and redesigned model of the Syscal Electrical resistivity meters. Its lightweight, modern and robust design makes it ideal for use in the field for easy data acquisition and deployment. The high power (up to 10000 V) unit has a large built in colour touchscreen display along with the manual keypad, for easier menu navigation and data visualization.
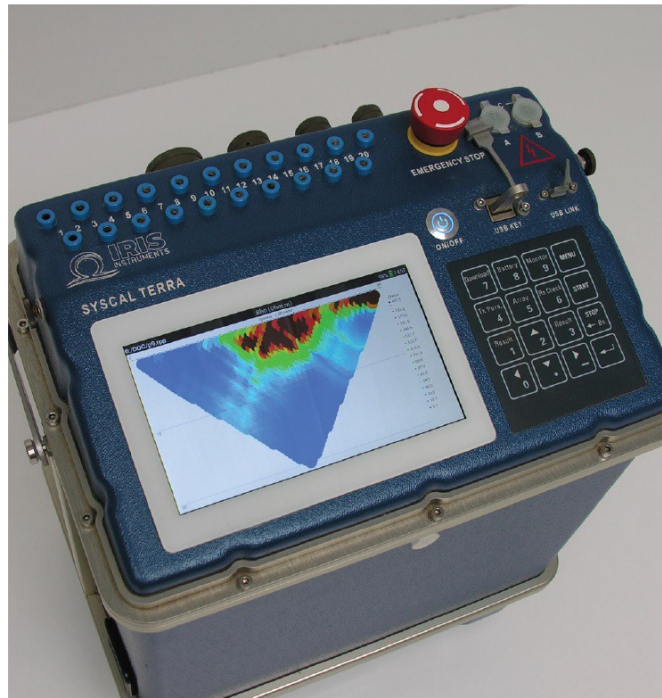
Fig 18: Top View of the Syscal terra unit including the colour display, keypad and ports (Image courteously provided by Iris Instruments)

The system uses 20 measurement channels, enabling faster runtimes to acquire Resistivity and Induced Polarisation (IP) data with improved resolution at deeper penetration depths; Both the IP and the resistivity measurements are collected in the "On time" injection cycle reducing the sampling time. Multiple Wenner-Schlumberger reciprocal or dipole-dipole configurations can be measured with the unit, useful when acquiring 3D datasets.

The unit runs on Li batteries which are stored in a lower compartment on the unit and can be easily removed, ideal for when transporting the goods internationally/ by courier. The LI batteries can then be stored in cabin baggage during transport, alternatively, both the Tx and Rx can be powered by external batteries in the field (12V car batteries).

The unit also enables the user to check system functionality with built in test procedures and test

plugs to check the Rx, Tx, Switching boards and test the external battery.

Dimensions (L x W x H)	45 cm x 37 cm x 24 cm
Weight	14.7 kg
GPS:	UTM Coordinates, Internal GPS
Memory and Temperature Range:	2Gb and USB ports for external memory (1Tb) ; -20°C to +70°C
Screen:	7 inches [480 x 800] color touch screen (can be deactivated if required)
Batteries:	Li batteries (4 x 96 Wh), if an external battery is plugged in instead the unit automatically recognizes it as an external unit.
Display:	Can View the real-time pseudosection of the data on demand
Tx Max Voltage, Power and Current:	800V in Switch mode and 1000 V in standard mode, 250W/1200W with an external AC/DC converter; 2.5 Amp
Rx Measurement channels:	20ch galvanic ally isolated

Table 1: Technical characteristics of the syscal Terra unit.

Surveys were collected using a Syscal Terra with a dipole dipole and multiple-gradient arrays on a transect line of 14.2 m composed of 72 stainless-steel electrodes spaced 0.2 m. Electrodes were hammered into the first few centimeters of the ground, looking for the best compromise to ensure electrical contact and point-like current injection. The inversion process of the acquired dataset has been performed with the ResIPy software, based on the R2/R3t codes based on Occam's inversion method.

4.3 Inverted Section Analysis via ResIPy Software for Synthetic and Real Dataset

The multiple-gradient Array and Dipole-Dipole Array techniques are frequently utilized in electrical resistivity surveys for subsurface investigations. While both methods offer insights into subsurface structures, their efficiencies in deeper regions remain an area of interest and contention. This study seeks to explore and compare the efficacy of these methods specifically in deeper subsurface layers.

The comparison was conducted through field surveys employing both the multiple-gradient Array and Dipole-Dipole Array configurations. Measurements were taken systematically at various depths to capture subsurface resistivity variations. The collected data were then processed and plotted to analyze the performance of each method at increasing depths.

(A) multiple-gradient array 2D sensitivity section (real dataset)
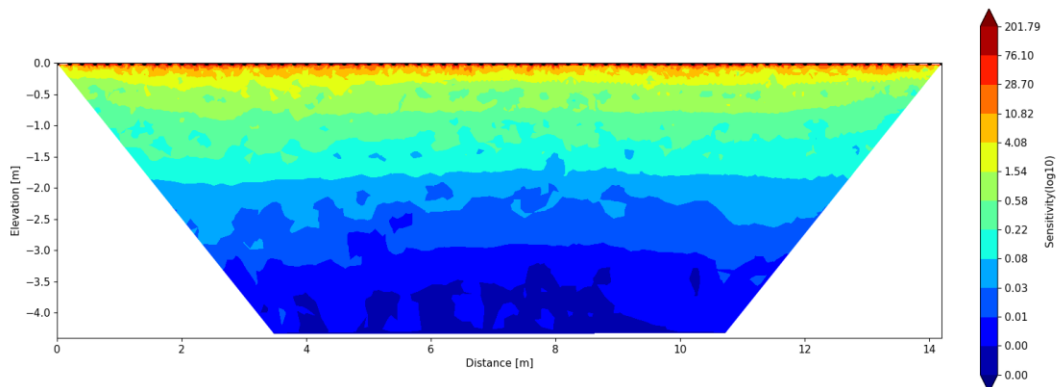
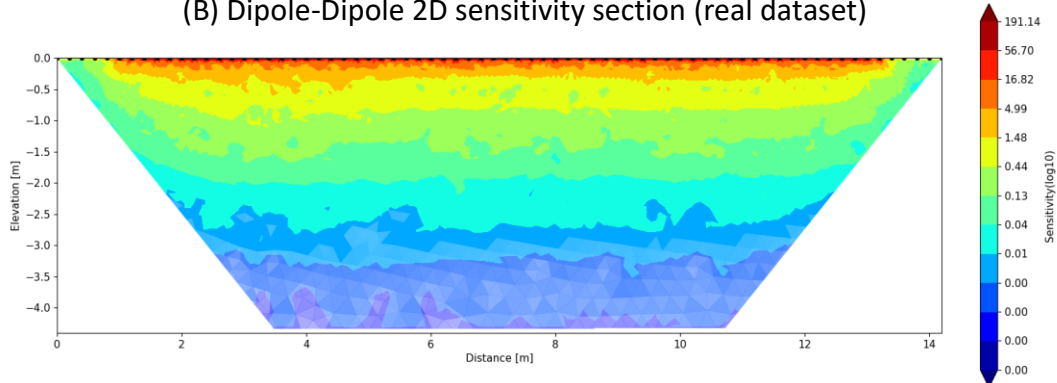(B) Dipole-Dipole 2D sensitivity section (real dataset)

Fig 19: Comparison of 2D Sensitivity Sections: multiple-gradient Array vs. Dipole-Dipole Configuration for Subsurface Investigations Related to Field Dataset.

(A) multiple-gradient array 2D inverted model (real dataset)

(B) Dipole-Dipole array 2D inverted model (real dataset)
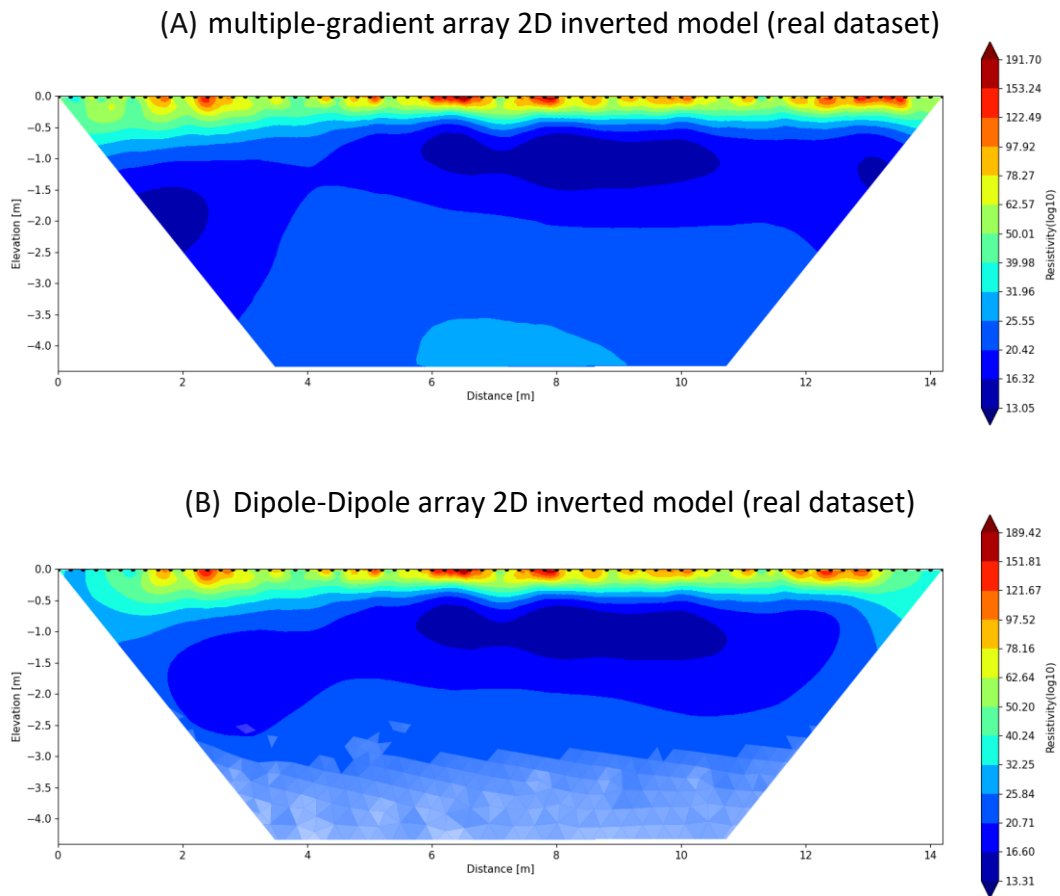

Fig 20: Comparison of 2D inverted models: multiple-gradient Array vs. Dipole-Dipole Configuration for Subsurface Investigations Related to Field Dataset.
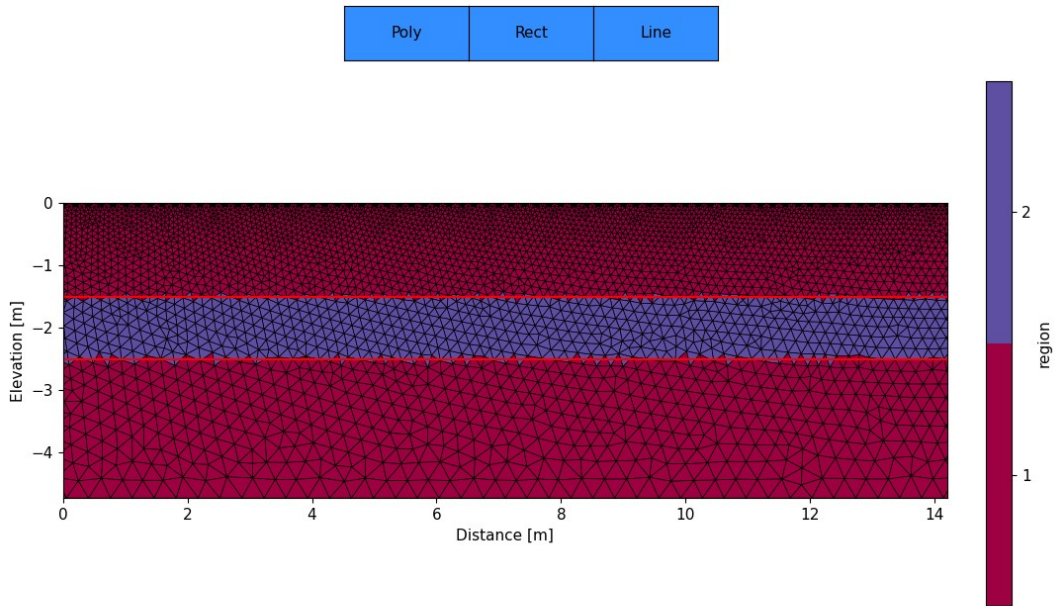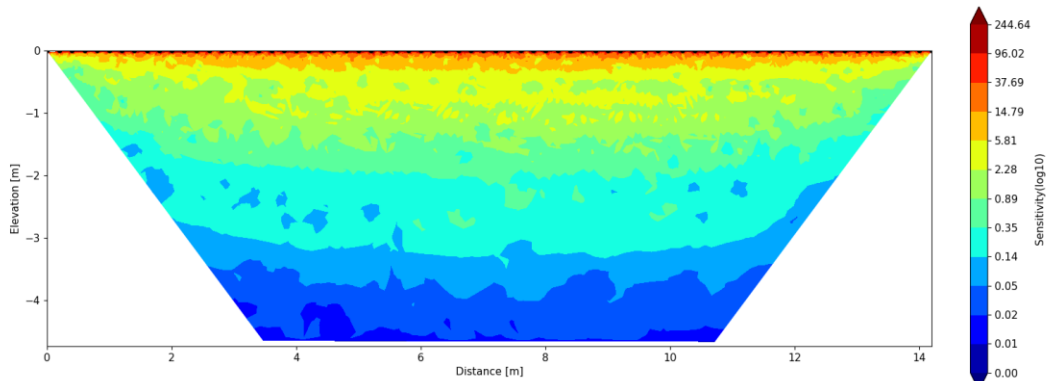
Fig 21: 2D Mesh Plot Displaying Contrasting Resistivity Layers: Conductive Layer (50 ohm.m) Positioned at 1.5 to 2.5m Depth Against Background Lithology (500 ohm.m).

(A) multiple-gradient array 2D sensitivity section (synthetic model)

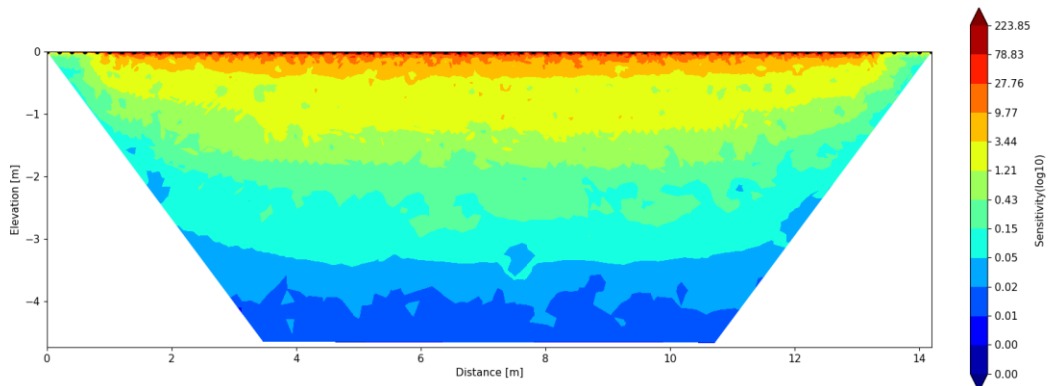(B) Dipole-Dipole 2D sensitivity section (synthetic model)

Fig 22: Comparative 2D synthetic sections: Synthetic Subsurface Investigations Using multiple-gradient Array vs. Dipole-Dipole Configuration.

(A) multiple-gradient array 2D inverted model (synthetic model)
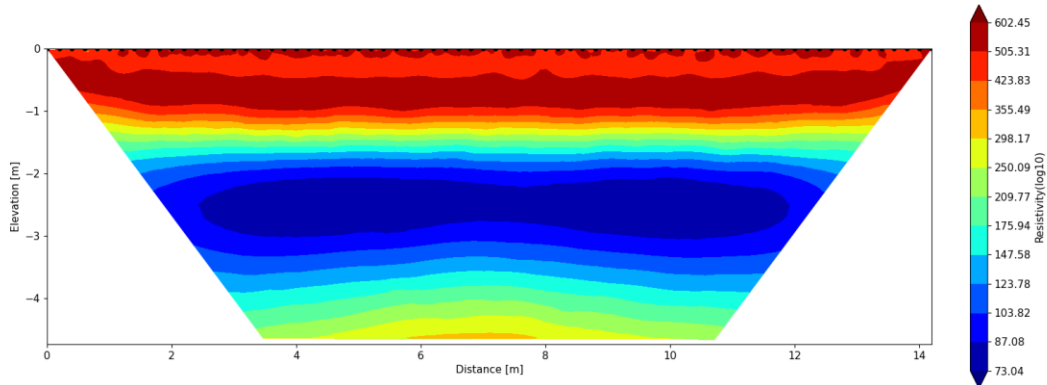
(B) Dipole-Dipole array 2D inverted model (synthetic model)
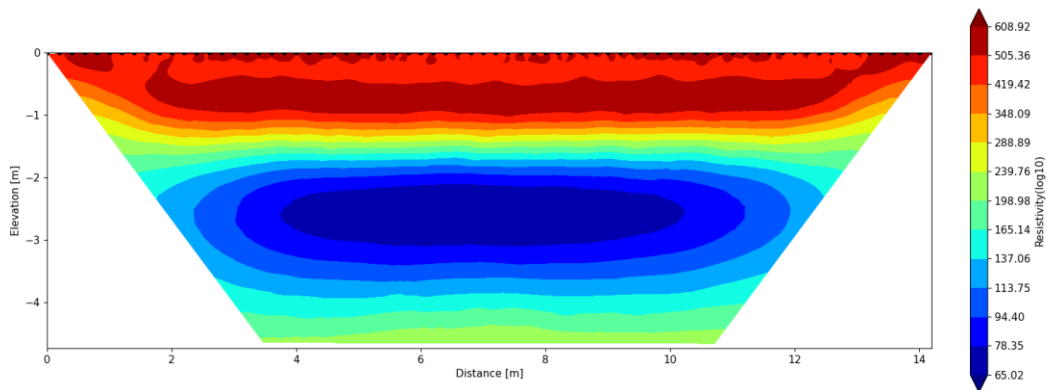
Fig 23: Comparative 2D inverted model: Synthetic Subsurface Investigations Using multiple-gradient Array vs. Dipole-Dipole Configuration.

The plotted data revealed significant differences in the efficiency of the multiple-gradient Array and Dipole-Dipole Array techniques as the depth increased. The multiple-gradient Array showcased superior performance in deeper subsurface layers, demonstrating more accurate and clearer delineation of resistivity contrasts compared to the Dipole-Dipole Array.

Conclusion

The comparative analysis conducted by this study underscores the remarkable advantages of the multiple-gradient array over the dipole-dipole array in subsurface investigations. Their study, encompassing various numerical models and field experiments, illuminated the distinct superiority of the gradient array, especially in terms of resolution and practical efficiency.

Across multiple numerical models, the gradient array with its multitude of current-electrode combinations emerged as a frontrunner in resolving subsurface structures. Field experiments further fortified this conclusion, affirming the gradient array's prowess in multichannel data acquisition—a facet where it outshone the Dipole-Dipole array by demonstrating significantly better resolution capabilities.

The practical advantages of the multiple-gradient array were equally compelling. The accelerated pace of measurement, facilitated by its multichannel surveying capability, revolutionized fieldwork logistics. In contrast to single-channel surveying that often led to substantial crew downtime, the multichannel gradient array streamlined the workflow, minimizing waiting periods and maximizing field crew productivity.

The significance of data density became apparent in our findings. The gradient array's ability to achieve higher data density was identified as a pivotal factor driving improved resolution. Remarkably, an increase in data density, achievable through multichannel data acquisition, significantly enhanced the resolution capabilities, emphasizing the merit of employing such methods.

Moreover, the higher data density offered redundancy, mitigating the risks associated

with data loss, such as skipped electrodes. This redundancy also empowered practitioners to edit out noisy data points without disproportionately compromising the quality of the inverted model—an advantage critical for ensuring the fidelity of the results.

The superiority of the multiple-gradient array extended beyond resolution and logistical efficiency. In scenarios involving more channels or longer electrode separations, it boasted better signal-to-noise levels compared to the dipole-dipole array, underscoring its versatility and adaptability across varying survey conditions.

Ultimately, the study conclusively advocated for the multiple-gradient array, particularly in multichannel resistivity imaging, attributing to its unequivocal advantages in resolution, data acquisition efficiency, noise handling, and signal-to-noise levels. Nonetheless, the choice of electrode array remains contingent upon the specific objectives of the investigation, prevailing site conditions, and logistical considerations.

References

Cassiani, G., Boaga, J., Barone, I., Perri, M.T., Deidda, G.P., Vignoli, G., Strobbia, C., Busato, L., Deiana, R., Rossi, M., Caputo, M.C., De Carlo, L. (2020). Chapter 3 Ground-based remote sensing of the shallow subsurface: Geophysical methods for environmental applications. DOI: 10.1016/B978-0-444-64177-9.00003-5

Binley, A., Kemna, A. (2005). Hydrogeophysics DC Resistivity and Induced Polarization Methods.

Befus, K.M. (2017). pyres: A Python Wrapper for Electrical Resistivity Modeling with R2. J. Geophys. Eng. DOI: 10.1088/1742-2140/aa93ad.

Binley, A. (2015). "Tools and Techniques: DC Electrical Methods." In: Treatise on Geophysics, 2nd Edition, G. Schubert (Ed.), Elsevier, Vol. 11, 233-259. DOI: 10.1016/B978-0-444-53802-4.00192-5. (Available from the author on request).

Binley, A., Kemna, A. (2005). "Electrical Methods." In: Hydrogeophysics by Rubin and Hubbard (Eds.), Springer, 129-156.

Blanchy, G., Saneiyan, S., Boyd, J., McLachlan, P., Binley, A. (2020). "ResIPy, an intuitive open-source software for complex geoelectrical inversion/modeling in 2D space." Computer & Geosciences, 137. DOI: 10.1016/j.cageo.2020.104423

Boyd, J., Blanchy, G., Saneiyan, S., Binley, A. (2019). "3D geoelectrical problems with ResIPy, an open-source graphical user interface for geoelectrical data processing." FastTIMES, 24.

LaBrecque, D.J., X. Yang (2001). "Difference Inversion of ERT Data: a Fast Inversion Method for 3-D In Situ Monitoring." Journal of Environmental and Engineering Geophysics, 6(2), 83-89.

LaBrecque, D.J., M. Miletto, W. Daily, A. Ramirez, E. Owen (1996). "The effects of noise on

Occam's inversion of resistivity tomography data." Geophysics, 61, 538-548.

Lowry, T., M.B. Allen, P.N. Shive (1989). "Singularity removal: A refinement of resistivity modeling techniques." Geophysics, 54, 766–774.

Morelli, G., D.J. LaBrecque (1996). "Advances in ERT modeling." European Journal of Environmental and Engineering Geophysics, 1, 171-186.

Oldenburg, D., Y. Li (1999). "Estimating depth of investigation in DC resistivity and IP surveys." Geophysics, 64(2), 403-416.

Befus, K.M., 2018. pyres: a Python wrapper for electrical resistivity modeling with R2. J. Geophys. Eng. 15, 338–346. https://doi.org/10.1088/1742-2140/aa93ad.

Benoit, S., Ghysels, G., Gommers, K., Hermans, T., Nguyen, F., Huysmans, M., 2018. Characterization of spatially variable riverbed hydraulic conductivity using electrical resistivity tomography and induced polarization. Hydrogeol. J. 27, 395–407. https://doi.org/10.1007/s10040-018-1862-7.

Binley, A., Kemna, A., 2005. DC resistivity and induced polarization methods. In: Hydrogeophysics. Springer, pp. 129–156.

Boyd, J., Blanchy, G., Saneiyan, S., Binley, A., 2019. 3D geoelectrical problems with ResIPy, an open-source graphical user interface for geoeletrical data processing. FastTIMES 24. Cockett, R., Kang, S., Heagy, L.J., Pidlisecky, A., Oldenburg, D.W., 2015. SimPEG: an open source framework for simulation and gradient based parameter estimation in geophysical applications. Comput. Geosci. 85, 142–154. https://doi.org/10.1016/j.cageo.2015.09.015.

Crook, N., Binley, A., Knight, R., Robinson, D.A., Zarnetske, J., Haggerty, R., 2008. Electrical resistivity imaging of the architecture of substream sediments. Water Resour. Res. 44 https://doi.org/10.1029/2008WR006968.

Flores Orozco, A., Williams, K.H., Kemna, A., 2013. Time-lapse spectral induced polarization imaging of stimulated uranium bioremediation. Surf. Geophys. 11, 531–544. https://doi.org/10.3997/1873-0604.2013020.

Geuzaine, C., Remacle, J.-F., 2009. Gmsh: a 3-D finite element mesh generator with builtin pre- and post-processing facilities. Int. J. Numer. Methods Eng. 79, 1309–1331. https://doi.org/10.1002/nme.2579.

Hunter, J.D., 2007. Matplotlib: a 2D graphics environment. Comput. Sci. Eng. 9, 90–95. https://doi.org/10.1109/MCSE.2007.55.

Johnson, T.C., Hammond, G.E., Chen, X., 2017. PFLOTRAN-E4D: a parallel open source PFLOTRAN module for simulating time-lapse electrical resistivity data. Comput. Geosci. 99, 72–80. https://doi.org/10.1016/j.cageo.2016.09.006.

Karaoulis, M., Revil, A., Tsourlos, P., Werkema, D.D., Minsley, B.J., 2013. IP4DI: a software for time-lapse 2D/3D DC-resistivity and induced polarization tomography.

Comput. Geosci. 54, 164–170. https://doi.org/10.1016/j.cageo.2013.01.008.

Koestel, J., Kemna, A., Javaux, M., Binley, A., Vereecken, H., 2008. Quantitative imaging of solute transport in an unsaturated and undisturbed soil monolith with 3-D ERT and TDR. Water Resour. Res. 44 https://doi.org/10.1029/2007WR006755 n/a–n/a.

LaBrecque, D.J., Yang, X., 2001. Difference inversion of ERT data: a fast inversion method for 3-D in situ monitoring. J. Environ. Eng. Geophys. 6, 83–89.

McLachlan, P.J., Chambers, J.E., Uhlemann, S.S., Binley, A., 2017. Geophysical characterisation of the groundwater–surface water interface. Adv. Water Resour. 109, 302–319. https://doi.org/10.1016/j.advwatres.2017.09.016.

Mewes, B., Hilbich, C., Delaloye, R., Hauck, C., 2017. Resolution capacity of geophysical

monitoring regarding permafrost degradation induced by hydrological processes. The Cryosphere 11, 2957–2974. https://doi.org/10.5194/tc-11-2957-2017.

Mwakanyamale, K., Slater, L., Binley, A., Ntarlagiannis, D., 2012. Lithologic imaging using complex conductivity: lessons learned from the Hanford 300 Area. Geophysics 77, E397–E409. https://doi.org/10.1190/geo2011-0407.1.

Nath, S.K., Shahid, S., Dewangan, P., 2000. SEISRES—a visual Cþþ program for the sequential inversion of seismic refraction and geoelectric data. Comput. Geosci. 26, 177–200.

Ntarlagiannis, D., Robinson, J., Soupios, P., Slater, L., 2016. Field-scale electrical geophysics over an olive oil mill waste deposition site: evaluating the information content of resistivity versus induced polarization (IP) images for delineating the spatial extent of organic contamination, pp. 418–426. https://doi.org/10.1016/j.jappgeo.2016.01.017, 135.

Oldenburg, D.W., Li, Y., 1999. Estimating depth of investigation in dc resistivity and IP surveys. Geophysics 64, 403–416.

Orozco, A.F., Kemna, A., Zimmermann, E., 2012. Data error quantification in spectral induced polarization imaging, pp. E227–E237. https://doi.org/10.1190/geo2010-0194.1, 77.

Pidlisecky, A., Knight, R., 2008. FW2_5D: a MATLAB 2.5-D electrical resistivity modeling code. Comput. Geosci. 34, 1645–1654.

Rücker, C., Günther, T., Wagner, F.M., 2017. pyGIMLi: an open-source library for modelling and inversion in geophysics. Comput. Geosci. 109, 106–123. https://doi.org/10.1016/j.cageo.2017.07.011.

Saneiyan, S., Ntarlagiannis, D., Ohan, J., Lee, J., Colwell, F., Burns, S., 2019. Induced polarization as a monitoring tool for in-situ microbial induced carbonate

precipitation (MICP) processes. Ecol. Eng. 127, 36–47. https://doi.org/10.1016/j.ecoleng.2018.11.010.

Saneiyan, S., Ntarlagiannis, D., Werkema, D.D., Ustra, A., 2018. Geophysical methods for monitoring soil stabilization processes. J. Appl. Geophys. 148, 234–244. https://doi.org/10.1016/j.jappgeo.2017.12.008.

Schlumberger, C., 1920. Etude sur la prospection electrique du sous-sol. Gauthier-Villars.

Uhlemann, S., Wilkinson, P.B., Maurer, H., Wagner, F.M., Johnson, T.C., Chambers, J.E., 2018. Optimized Survey Design for Electrical Resistivity Tomography: Combined Optimization of Measurement Configuration and Electrode Placement 36.

Vanella, D., Cassiani, G., Busato, L., Boaga, J., Barbagallo, S., Binley, A., Consoli, S., 2018. Use of small scale electrical resistivity tomography to identify soil-root interactions during deficit irrigation. J. Hydrol 556, 310–324. https://doi.org/10.1016/j.jhydrol.2017.11.025.

Ward, A.S., Gooseff, M.N., Singha, K., 2013. How does subsurface characterization affect simulations of hyporheic Exchange? Ground Water 51, 14–28. https://doi.org/10.1111/j.1745-6584.2012.00911.x.

Whalley, W.R., Binley, A., Watts, C.W., Shanahan, P., Dodd, I.C., Ober, E.S., Ashton, R.W., Webster, C.P., White, R.P., Hawkesford, M.J., 2017. Methods to estimate changes in soil water for phenotyping root activity in the field. Plant Soil 415, 407–422. https://doi.org/10.1007/s11104-016-3161-1.